Modular MEMS-Based Optical Cross-Connect With Large Port-Count

J. I. Dadap, P. B. Chu, I. Brener, C. Pu, C. D. Lee, K. Bergman, N. Bonadeo, T. Chau, M. Chou, R. Doran, R. Gibson, R. Harel, J. J. Johnson, S. S. Lee, S. Park, D. R. Peale, R. Rodriguez, D. Tong, M. Tsai, C. Wu, W. Zhong, E. L. Goldstein, L. Y. Lin, and J. A. Walker

***Abstract*—We describe and demonstrate a modular microelectromechanical systems (MEMS)-based optical cross-connect (OXC) architecture. The OXC port count increases modularly by adding new optical modules, and a maximum cross-connectivity of $\sim 350 \times 350$ can be achieved in the current design. Each optical module has 16 ports with closed-loop servo-controlled MEMS mirrors. Using a prototype OXC system, mounted in a standard telecommunications equipment bay comprising optical modules, folding mirrors, and other optical elements, we demonstrate switching times of less than 10 ms, excellent optical power stability of less than $\pm$0.15-dB variation, and immunity to stochastic vibrations. An automatic power peak-up process is performed when the power falls below 0.5 dB off the maximum coupled power for any connection.**

***Index Terms*—Microelectromechanical systems (MEMS), modular switching, optical cross-connect (OXC), optical fiber communications, optical switching.**

I. Introduction

OVER THE past few years, microelectromechanical systems (MEMS) technology has emerged as a major candidate for building high port-count optical cross-connect (OXC) switches suitable for deployment in the core-transport networks [1]. The switch fabrics present in these high port-count crossconnects typically require hundreds of fibers, lenses, and MEMS silicon tilting mirrors [2], [3] precisely aligned in a three-dimensional configuration, and in addition, hundreds or thousands of electrical signals may be needed to be routed to control the MEMS mirrors. The popular approach in a MEMS-based OXC makes use of large monolithic mirror chips, fiber bundles, and lens arrays, which requires stringent alignment tolerances of a few micrometers (e.g., for the fibers and lenses) and tilting accuracies of tens of μrad in order to keep the excess optical loss to within 1 dB. Although the monolithic approach may simplify the packaging complexity of the OXC, its drawbacks are numerous. 1) Poor component yield will increase the cost-per-port, limit the array size, and thus, the overall port count. 2) Since these massive components must be factory installed and aligned, such a system requires high installation and replacement cost even if only a limited number of ports are needed initially. 3) A rigidly and permanently assembled system eliminates the possibility of component repair or replacement during service. Hence, to reduce the chance of a complete switch replacement during service, an overbuilt of the component arrays and associated electronics may be necessary, which may further drive up the cost-per-port, and may increase the insertion loss.

To solve these challenges, we developed a modular optical switch architecture. In a modular $N \times N$ switch architecture, where $2N$ is the total number of ports (input+output), the OXC is composed of several identical switch modules. Each module is comprised of $k(\ll N)$ ports. Each port consists of a fiber, a MEMS mirror, lenses, and an associated angle-sensing scheme. A modular architecture has a number of distinct benefits. 1) There is no port-yield bottleneck since each port is built from tested components and can be optimized individually. 2) Since each module contains a small number of ports, it can be built with relative ease. In addition, the assembly of the whole switch comprising an array of modules in a card cage and an optical chassis, is very similar to that of a standard communications equipment, and may be achieved with less difficulty compared to a switch fabric with huge monolithic component arrays. 3) The system capacity can be increased by adding new modules instead of installing a whole switch fabric as in a monolithic approach, thus, reducing startup cost and enabling pay-as-you-grow cost structure. 4) The system can allow in-service installation and replacement of individual modules instead of the whole switch fabric. For the last point, however, maintaining immunity to stochastic vibrations during in-service module installation or replacement is essential. We have, therefore, employed closed-loop servo control of the MEMS mirrors for long-term mechanical and electrical stability, and for its ability to provide extended mirror switching angles and faster switching times in contrast to open-loop control [4].

II. Description of the Modular System

The basic switch fabric is composed of arrays of identical 16-port module assemblies, shown schematically in Fig. 1. Each module resembles a large circuit board with the necessary mechanical structure to enable insertion and securing into a given slot of a card cage. It also contains a fiber-management spool, optical and electrical connectors, and support electronics built into the circuit board. Each optical port unit is comprised of a lens fused to the tip of the fiber, a folding mirror, a MEMS mirror, and a collimating lens. The fused lens serves to reduce the NA of the fiber from 0.13 to 0.07 in order to provide sufficient space between the optical components. The optimal relative distances between the fused lens, MEMS mirror, and col-

Manuscript received May 28, 2003; revised July 18, 2003.

The authors are with Tellium Inc., Oceanport, NJ 07757 USA (e-mail: dadap@cumsl.msl.columbia.edu; cpu@ieee.org).

Digital Object Identifier 10.1109/LPT.2003.819748

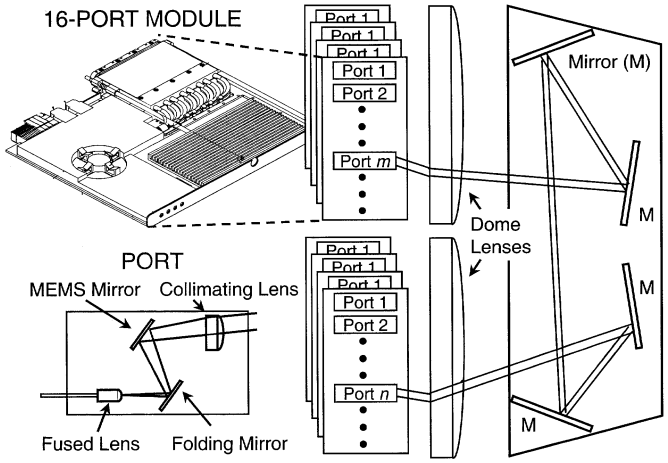

Fig. 1. Schematic of modular optical system.

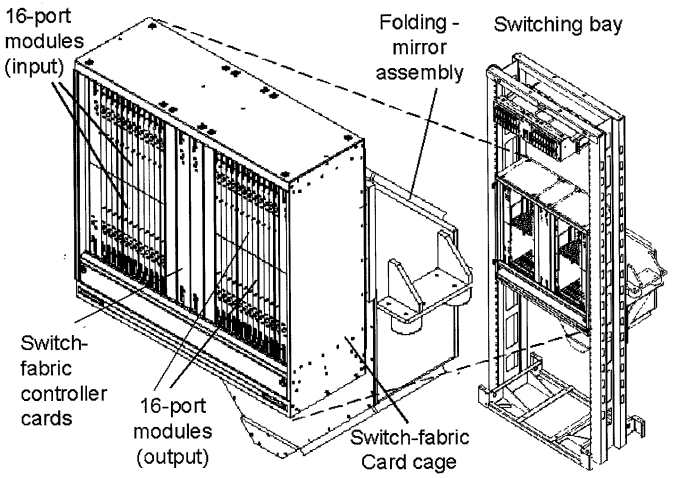

Fig. 2. Mechanical design of modular switch fabric.

limating lens ($f = 18$ mm), are determined such that the minimum beam waist position is closest to or located at a distance of 1 m from the port, corresponding to one half of the total path length of 2 m. This is accomplished through minor adjustments of the collimating lens position while monitoring the beam diameter at various locations along the beam path. This procedure limits any adverse effects of the variation of focal lengths of the lenses as well as the MEMS mirror curvature (focusing) radius, typically around $\sim$20 cm.

Outside of the optical units, two dome lenses ($f = 2$ m), each being large enough to cover the entire plane of the input or output port arrays, are added to the optical path in close proximity to the collimating lenses. This optical geometry provides invariance of the connection angles between any arbitrary port on one side (input or receiving) of the OXC to a specific port on the opposite side of the OXC. As an example, for ideal optical components and alignment, if all input mirrors are tilted in the same direction all input port beams will be redirected to one unique spot on the receiving dome lens. The starting lookup table for the connection angles is drastically simplified by making use of this strategy.

An auxiliary MEMS tilt angle-sensing system (not shown) is incorporated into each port, utilizing either optical or capacitive sensing. Here, we report data obtained using the former, which employs a dichroic beam splitter between the MEMS mirror and the collimating lens. It redirects an out-of-band laser into a position-sensitive detector while providing negligible loss at the copropagating data wavelength of 1310 nm. The theoretical optical loss for the designed optical configuration is 2.5 ± 0.5 dB for all possible connections, which takes into account all possible optical loss mechanisms including those due to the MEMS mirror etch holes, spring area, and variations in MEMS curvature radius (20–60 cm). For the prototype mirrors, where only 85% of the available area is gold coated, we have measured losses of 6.0 $\pm$ 1.0 dB, close to the predicted value of $\sim$5.5 dB.

The mechanical design of the OXC is illustrated in Fig. 2. From the front view, the card cage is divided into two sides, two rows of 12 vertical slots for 24 input modules on the left and a symmetric structure for 24 output modules on the right. The two sides are separated by additional slots for switch-fabric controller cards. Attached to the back of the card cage is an optical chassis with four folding mirrors (denoted as M in Fig. 1), directing light from input modules on one side to the output modules on the opposite side. The card cage and the optical chassis are mounted on a standard wide-bay rack via four dampers that provide isolation from mechanical vibrations.

Given that the vertical and horizontal pitch of the optical ports are 8.5 and 12.0 mm, respectively, a fully populated card cage would support a 384 (16 times 24) by 384 strictly nonblocking switch. The maximum measurable mechanical tilt is $\pm 7^\circ$, limited by the angle-sensing optics. After allocating about $\pm 3^\circ$ to compensate for component misalignment and packaging tolerances, we may realize, conservatively, 348 by 348 valid connections with $\pm 4^\circ$ of MEMS tilting. The maximum port count may be increased by reducing the optical pitch, increasing the MEMS tilt angles, improving manufacturing tolerance, and optimizing the lens design. The scaling of the port count to higher numbers is limited chiefly by the port size and, to a lesser extent, crosstalk. The crosstalk of the system is expected to be very low because of the large optical beam waist ($>$1 mm). For the demonstration described here, we populated our prototype OXC with six optical modules, which provided a total of four transmitting and four receiving ports. These modules were then moved to different locations to simulate large-port count OXC switching, to measure parameters such as switching time, and to test the peak-up algorithm described below.

III. MEMS and Control System

The MEMS mirrors used in this work are double-gimbaled tilting mirrors made of 10-μm-thick single-crystal silicon with radius from 400 to 450 μm [5]. Suspended by torsional springs, the mirrors are designed to have resonant frequency at zero deflection angle typically between 300 and 400 Hz (both axes), with Q (in air) of $\sim$3 to 5 for both axes. The mirrors are coated with a thin adhesion and 700-Å-thick gold layers. The MEMS mirrors are electrostatically actuated by quadrant electrodes underneath the mirrors with less than 85 V, using a closed-loop servo control system that provides immunity to stochastic vibrations, long-term mechanical and electronic drift, and enables a large mechanical tilt angle ($\pm 9^\circ$) and fast switching time ($<$10 ms). Hermetic sealing will be required

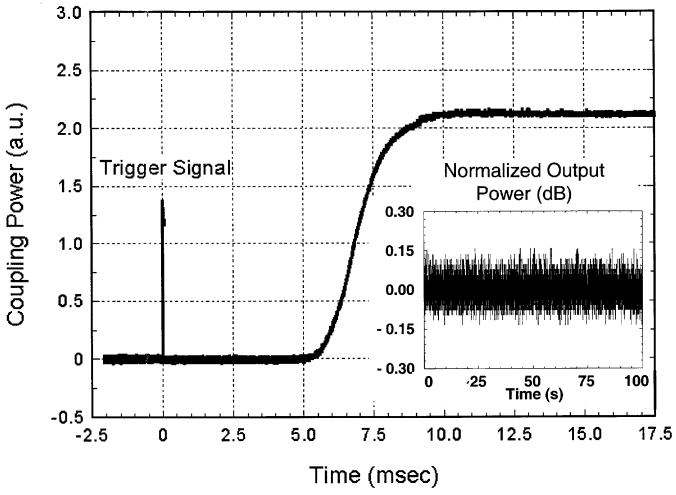

Fig. 3. Typical OXC event. The switching time is measured from the trigger pulse. Inset: fiber-coupled power stability measurement over 100 s.

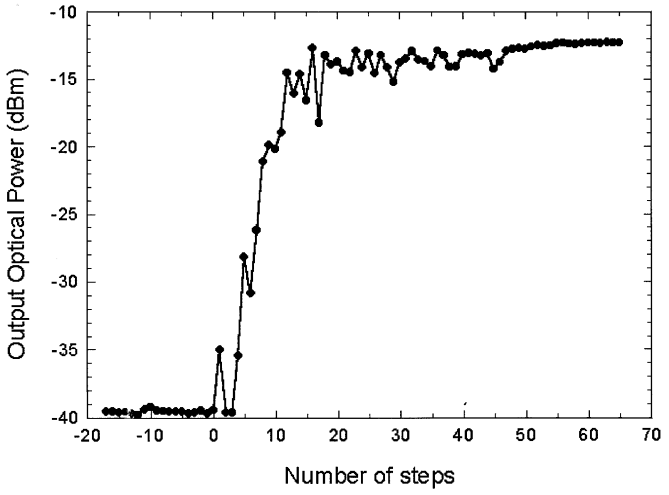

Fig. 4. Typical automatic power-peaking event starting from ∼30 dB below peak power coupling.

for the MEMS mirrors in a real product, but for this prototype demonstration we used unsealed mirrors.

The nonlinear controller is based on a new torque-to-voltage conversion technique [4] and classic linear controller techniques with full-state feedback, state estimator, and reference input with feed-forward [6]. The controller is implemented using a 100-MHz 600FLOPS (32-b floating point) digital signal processor (DSP) with interfaces to multiple analog-to-digital–digital-to-analog converters. After code optimization, a single DSP could servo eight mirrors with a sampling rate of 20 kHz (or 16 mirrors at 10 kHz). Long-term (∼10 h) mechanical tilt angular noise of less than 150 μrad is achieved. The servo-control also provides the necessary noise immunity for in-service module insertion into the system card cage. Although vibration isolation for this system was not systematically characterized, manual perturbation to the chassis (e.g., applying an impulsive force, opening and closing card cage) did not result in any measurable power drop.

IV. Results and Discussion

Fig. 3 shows a typical switching event from the moment the command is received by the DSP controller until the peak power coupling is achieved. The switching time, defined as the period between the onset of the command and the power coupling reaching 90% of its peak, is less than 8 ms even when mirrors tilt between large extreme angles, e.g., from -5° to 5°. A recording of the fiber-to-fiber coupled power (inset) over a span of 100 s under normal operation at room temperature reveals power fluctuations to be within ± 0.15 dB, which is due to the excellent noise rejection and pointing stability provided by the closed-loop control.

Coupling power for each connection is maximized using an optimization method based on a four-dimensional peak-search algorithm. The four dimensions arise from the two tilting axes of both input and output mirrors. This peak search algorithm is used for two purposes. 1) During operation, the algorithm actively checks *all* connections for slow power drifts and performs small angular corrections if the power falls by more than 0.5 dB from maximum coupling. 2) This algorithm is used to find the initial angles for a connection during the installation of new switching modules. When a switching module is plugged into position and the MEMS mirrors are actuated according to the initial look-up table, the coupled power could be in the range of -30 to -40 dB off its peak. Fig. 4 shows a typical automatic power-peaking process that takes less than 70 steps to reach peak power from around 30 dB below peak. Each step indicates a concerted tilting of corresponding transmitting and receiving mirrors. Power measurements for the peak-up algorithm were sampled at 1-kHz rate. The theoretical speed of this peak-up process is limited by the photodiode efficiency, the power resolution (typically ∼0.05 dB), and the mechanical response of the mirrors for small-angle switching.

V. Summary

We have demonstrated a modular architecture for an OXC using MEMS mirrors running under fully closed-loop servo control. Switching times of less than 10 ms and mirror angular noise of less than 150 μrad are achieved.

References

[1] L. Y. Lin, E. L. Goldstein, and R. W. Tkach, "On the expandability of free-space micromachined optical cross connects," *J. Lightwave Technol.*, vol. 18, pp. 482–489, Apr. 2000.

[2] D. J. Bishop, C. R. Giles, and G. P. Austin, "The Lucent LambdaRouter: MEMS technology of the future here today," *IEEE Commun. Mag.*, vol. 40, pp. 75–79, Mar. 2002.

[3] P. B. Chu, S.-S. Lee, and S. Park, "MEMS: the path to large optical crossconnects," *IEEE Commun. Mag.*, vol. 40, pp. 80–87, Mar. 2002.

[4] I. Brener *et al.*, "Nonlinear servo control of MEMS mirrors and their performance in a large port-count optical switch," in *OFC 2003*, Atlanta, GA, Mar. 2003, pp. 385–386.

[5] S. Blackstone and T. J. Brosnihan, "SOI MEMS technologies for optical switching," in *Proc. IEEE/LEOS Int. Conf. Optical MEMS 2001*, Okinawa, Japan, 2001, p. 35.

[6] G. F. Franklin, J. D. Powell, and M. L. Workman, *Digital Control of Dynamic Systems*. Reading, MA: Addison-Wesley, 1998, pp. 323–325.